Engineering and Technology Journal e-ISSN: 2456-3358

Volume 09 Issue 07 July-2024, Page No.- 4550-4554

DOI: 10.47191/etj/v9i07.25, I.F. – 8.227

Temperature-Dependent XAFS Debye-Waller Factor of Molybdenum Metal Calculated using Anharmonic Correlated Einstein Model

Trinh Phi Hiep

Department of Education, Tan Trao University, Tuyen Quang, Vietnam

ABSTRACT: Temperature-dependent X-ray absorption fine structure (XAFS) Debye-Waller (DW) factor of molybdenum (Mo) metal has been studied under the influence of thermal disorders. This factor is calculated in simple and explicit forms using the classical anharmonic correlated Einstein (CACE) model, which is developed from the correlated Einstein model based on the anharmonic effective potential and the classical statistical theory. The numerical results of Mo in the temperature range from 0 to 800 K are in good agreement with those obtained by the other theoretical models and experiments at several temperatures. The analytical results show that the CACE model is suitable for analyzing the experimental XAFS DW factor of Mo from above the correlated Einstein temperature to before the melting temperature.

KEYWORDS: XAFS DW factor, CACE model, thermal disorders, crystalline molybdenum

1. INTRODUCTION

Recently, the X-ray absorption fine structure (XAFS) has been developed into a powerful technique because it can be widely used to determine many thermodynamic properties and structural parameters of materials [1]. However, thermal disorders will distort the arrangement order of atoms and their interaction in the crystal, so thermal disorders are very sensitive to the XAFS signal [2]. As a result, if the effect of thermal disorders is not considered in the anharmonic XAFS data analysis, it will provide misinformation about the thermodynamic properties of materials [3]. The anharmonic XAFS Debye-Waller (DW) factor $\mathrm{W}(T,k)$ can describe the thermal disorder in the neighbor distance and determines the anharmonic XAFS amplitude reduction, so it is an important parameter in the investigation of the anharmonic XAFS signal [4].

Nowadays, molybdenum (Mo) metal is considered an alloying agent in structural and stainless steels because of its strength, corrosion resistance, and ability to retain shape and perform at high temperatures. [5]. This metal is produced as an alloying agent in various stainless steels and structures and is used in wear-resistant welding rods to increase rust resistance mechanical durability, help ease machining, and resist corrosion [6]. Meanwhile, the experimental XAFS signal of Mo at 293 K, 323 K, 373 K, 423 K, 473 K, 523 K, and 573 K was measured at the Synchrotron Radiation Siberian Center (SRSC), Russia, by Pirog *et al.* [7].

Currently, a classical anharmonic correlated Einstein (CACE) model has been applied to effectively treat the anharmonic XAFS parameters of metals [8]. This model has the advantage that the expressions of the anharmonic XAFS parameters are obtained in explicit and simple forms, so it is very convenient to analyze anharmonic XAFS data in the range of temperatures not too low [9]. Still, it has not yet been used to analyze the anharmonic XAFS DW factor of Mo. Therefore, investigating the temperature-dependent XAFS Debye-Waller factor of Mo based on the CACE model will be necessary for the experimental XAFS data analysis.

2. FORMALISM AND CALCULATION

The *K*-edge XAFS signal includes a non-Gaussian disorder for a given scattering path is expressed in terms of a canonical average of all distance-dependent factors by [10,11]

$$\chi(k,T)=\frac{Ne^{-2k^2\sigma^2(T)}f(k)}{kR^2(T)}\sin\left[2kR(T)+\delta(k)\right], \quad (1)$$

where k is the wave number of photoelectron, N is the number of neighboring atoms, $f(k)$ and $\delta(k)$ characterizes scattering parameters of the photoelectron, $\sigma^2(T)$ is the mean-square relative displacement (MSRD) or second XAFS cumulant, and $R(T)$ is the distance between atoms.

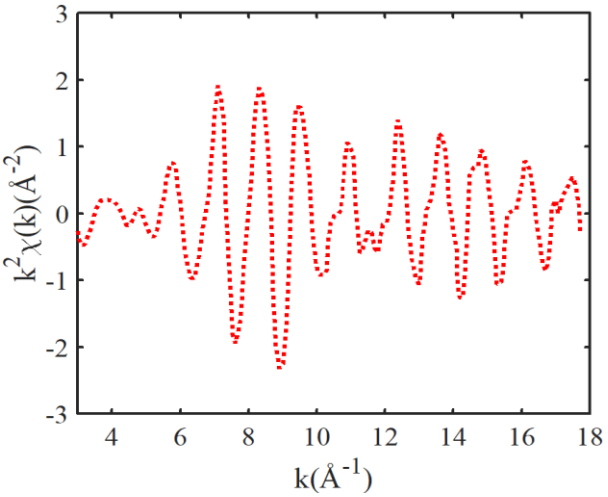

Fig. 1. The anharmonic XAFS signal of Mo were extracted from the experiments [7].

In analyzing the anharmonic XAFS signal as shown in Fig. 1, the anharmonic XAFS Debye-Waller (DW) factor $\mathrm{W}(T,k)$ is determined as follows [12,13]:

$$\mathrm{W}(T,k)=\exp\left\{-2k^2\sigma^2(T)\right\}, \quad (2)$$

$$\sigma^2(T)=\left\langle\left(r-\langle r\rangle\right)^2\right\rangle=\left\langle\left(x-\langle x\rangle\right)^2\right\rangle=\left\langle x^2\right\rangle-\langle x\rangle^2, \quad (3)$$

where the second XAFS cumulant $\sigma^2(T)$ can is explicitly related to low-order moments of true RD function, the angular bracket $\langle\ \rangle$ is the thermal average, x is the deviation distance between the backscattering and absorbing atoms, and r is the instantaneous bond length between atoms.

To determine the thermodynamic parameters of a system, it is necessary to specify its anharmonic effective (AE) potential and force constants [14]. The AE potential in the relative vibrations of backscattering (1) and absorbing (*2*) atoms can be calculated from the pair interaction (PI) potential [15]:

$$V_{eff}=V(x)+\sum_{i=1,2}\sum_{j\neq 1,2}V\left(\varepsilon_i x\hat{R}_{12}\hat{R}_{ij}\right),\ \varepsilon_i=\frac{\mu}{M_i}, \quad (4)$$

where $\mu=M_1M_2/(M_1+M_2)$ is the reduced mass of the backscatter with masse M_1 and absorber with masse M_2, sum i is the over backscatter ($i=1$) and absorber ($i=2$), the sum j is over the nearest neighbors, $\hat{R}$ is a unit vector, $V(x)$ is a PI potential of these atoms, $V\left(\varepsilon_i x\hat{R}_{12}\hat{R}_{ij}\right)$ express the contribution of nearest-neighbor atoms to $V(x)$.

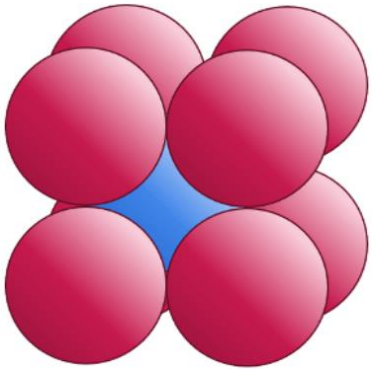

Fig. 2. The crystalline structure of Mo.

A body-centered cubic (BCC) structure of Mo is shown in Fig. 2. This structure has similar atoms at one center and eight corners of a cube, so each atom has a mass of *m*, and each unit cell contains two atoms [16]. After using structural characteristics, the AE potential of Fe is calculated from Eq. (4) and is written as

$$V_{eff}(x)=V(x)+V(0)+2V(-x/2)+6V(-x/6)+6V(x/6) \quad (5)$$

.

Usually, the Morse potential can validly determine the PI potential of the crystals [17]. If this potential is expanded up to the three orders around its minimum position, it can be written as

$$V(x)=D\left(\mathrm{e}^{-2\alpha x}-2e^{-\alpha x}\right)\cong -D+D\alpha^2x^2-D\alpha^3x^3+7D\alpha^4x^4/12,\ x=r-r_0 \quad (6)$$

,

where *D* is the dissociation energy, α is the width of the potential, and r_0 is the equilibrium bond length between atoms.

The result of AE potential can be obtained from Eq. (5) using Morse potential in Eq. (6). If ignoring the overall constant, it is presented in the form:

$$V_{eff}(x)=k_{eff}x^2/2-k_3x^3+k_4x^4, \quad (7)$$

where k_{eff} is the effective force constant, and k_3 and k_4 are anharmonic force constants, which are not the temperature-dependent and are written as

$$k_{eff}=\frac{11}{3}D\alpha^2,\quad k_3=\frac{3}{4}D\alpha^3,\quad k_4=\frac{1715}{2592}D\alpha^4, \quad (8)$$

The CACE model is derived from the correlated Einstein model using the AE potential and classical statistical theory [8]. In this model, each atomic thermal vibration can be treated as a phonon and characterized via the correlated Einstein temperature θ_E and frequency ω_D [18]. These parameters of Fe can be defined from the effective force constant as follows:

$$\omega_E = \sqrt{\frac{k_{eff}}{\mu}} = \alpha\sqrt{\frac{22D}{3m}}, \quad \theta_E = \frac{\hbar\omega_E}{k_B} = \frac{\hbar\alpha}{k_B}\sqrt{\frac{22D}{3m}}, \tag{9}$$

where $\hbar$ is the reduced Planck constant and k_B is the Boltzmann constant.

In the classical-statistical limit, the moments $\langle x^k \rangle$ can be determined by evaluating the thermal average in the third-order approximation [19]:

$$\langle x^k \rangle = \frac{\int_{-\infty}^{\infty} x^k \exp\left[-\frac{V_{eff}(x)}{k_B T}\right] dx}{\int_{-\infty}^{\infty} \exp\left[-\frac{V_{eff}(x)}{k_B T}\right] dx} \approx \frac{\int_{-\infty}^{\infty} x^k \exp\left[\frac{-k_0 x^2}{2k_B T}\right]\left[\sum_{n=0}^{3}\frac{1}{n!}\left(\frac{k_3 x^3 - k_4 x^4}{k_B T}\right)^k\right] dx}{\left(\frac{2\pi k_B T}{k_0}\right)^{1/2}\left[1+\frac{3(k_B T)}{k_0^2}\left(\frac{5k_3^2}{2k_0}-k_4\right)\right]}. \tag{10}$$

The temperature-dependent general expressions of the MSRD in the CACE model were calculated using Eqs. (3) and (10) by Stern *et al*. [19]. Substituting the expressions of local force constants k_{eff}, k_3, and k_4 of Fe in Eq. (8) into this expression of the MSRD, we obtain the following result:

$$\sigma^2(T) \approx \frac{3k_B T}{11D\alpha^2}\left(1-\frac{5743k_B T}{31944D}\right) \approx \frac{3k_B T}{11D\alpha^2}. \tag{11}$$

Substituting this cumulants into the Eq. (2) to calculate the temperature-dependent XAFS DW factor of Mo, we obtain the following result:

$$W(T,k) = \exp\left\{-\frac{6k_B T}{11D\alpha^2}k^2\right\}. \tag{12}$$

Thus, the CACE model has been extended to calculate the temperature-dependent XAFS DF factor of Mo efficiently. The expressions obtained using this model can satisfy all their fundamental properties in temperature dependence.

3. RESULT AND DISCUSSION

In this section, the numerical results of Mo are calculated using the CACE model based on the obtained expressions in Secs. 2 and their physical parameters, which are the atomic mass $m = 95.94$ u [20] and Morse potential parameters $D = 0.8032$ eV and $\alpha = 1.5079$ Å^{-1} [17]. We calculate using Eqs. (8)-(9) and obtain the local force constants $k_{eff} \approx 6.70$ eVÅ^{-2}, $k_3 \approx 2.07$ eVÅ^{-3}, and $k_4 \approx 2.75$ eVÅ^{-4}, the correlated Einstein frequency $\omega_E \approx 3.66\times10^{13}$ Hz, and the correlated Einstein temperature $\theta_E \approx 279.52$ K. Meanwhile, the respective values obtained from the experimental data are $k_{eff} \approx 7.5\pm0.9$ eVÅ^{-2}, $k_3 \approx 3.0\pm0.8$ eVÅ^{-3}, $k_4 \approx 2.2\pm3.1$ eVÅ^{-4}, $\omega_E \approx 3.47\pm0.16\times10^{13}$ Hz, and $\theta_E \approx 264.8\pm12.0$ K [7]. Our results do not differ much from the experimental values, especially regarding the correlated Einstein frequency and temperature.

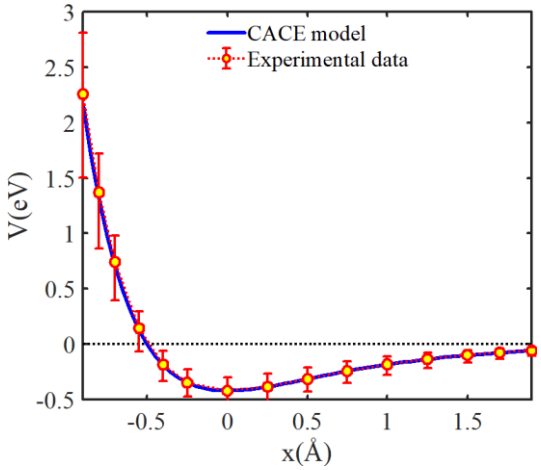

Fig. 3. The position-dependent Morse potential of Mo is obtained from the CACE model and experimental data [7].

The Morse potential $V(x)$ of Mo in the position dependence is represented in Fig. 3. Herein, our obtained result is calculated from Eq. (6), and the obtained result using the experimental data is calculated from Eq. (6) with the experimental Morse potential parameters $D = 0.75\pm0.13$ eV and $\alpha = 1.44\pm0.20$ Å^{-1} [7]. It shows that our results obtained using the CACE are satisfied with those obtained from experimental data error bars [7], especially at positions near the minimum position of these potentials. Also, the influence of anharmonic effects on the Morse potential is significant.

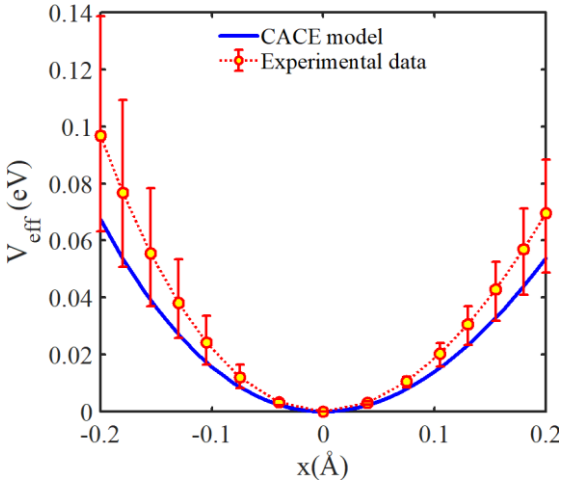

Fig. 4. The position-dependent AE potential of Mo is obtained from the CACE model and experimental data [7].

The position dependence of the AE potential $V_{eff}(x)$ of Mo in the position range from - 0.2 to 0.2 Å is represented in

Fig. 4. Our obtained result using the CACE model is calculated by Eqs. (7)-(8), while the experimental result is obtained from Eq. (7) with the above experimental values of local force constants [7]. Our result agrees better with those obtained from the experiment with error bars [7], especially at positions far from the minimum position. Moreover, the influence of anharmonic effects on the AE potential is stronger at positions further away from the minimum position of this potential. Note that our results of the Morse and AE potentials are similar to those obtained from the quantum anharmonic correlated Einstein (QACE) [21] and anharmonic correlated Debye (ACD) [22] models. It is because they are all calculated using Eq. (7) with similar values of the local force constants and Morse potential parameters.

The temperature dependence of the second XAFS cumulant $\sigma^2(T)$ of Mo in a range from 0 K to 900 K is represented in Fig. 5. Our obtained result using the CACE model is calculated by Eq. (11). It can be seen that our results are in agreement with those obtained using the QACE (only at the high temperatures) [21] and the ACD [22] models and experiment [7]. For example, the obtained results using the CACE, QACE model, ACD model, and experiment at $T =$ 373 K and 573 K are $\sigma^2 \approx 4.8\times10^{-3}$ Å^2 and $\sigma^2 \approx 7.4\times10^{-3}$ Å^2, $\sigma^2 \approx 5.1\times10^{-3}$ Å^2 and $\sigma^2 \approx 7.6\times10^{-3}$ Å^2[21], $\sigma^2 \approx 5.2\times10^{-3}$ Å^2 and $\sigma^2 \approx 7.5\times10^{-3}$ Å^2 [22], and $\sigma^2 \approx 4.6\times10^{-3}$ Å^2 and $\sigma^2 \approx 7.0\times10^{-3}$ Å^2 [7], respectively.

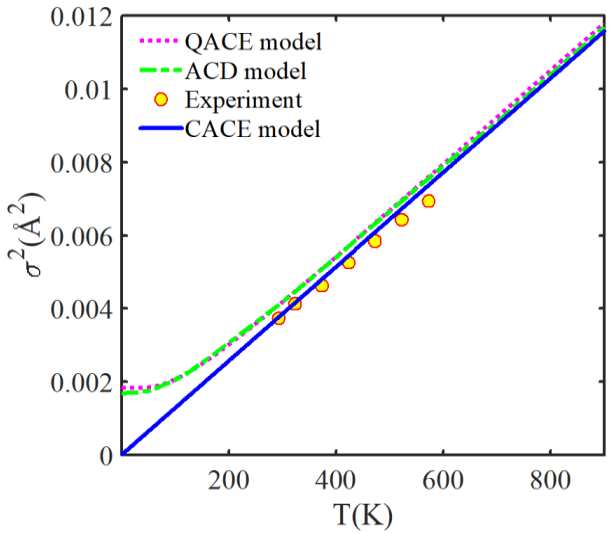

Fig. 5. Temperature-dependent second XAFS cumulants of Mo is obtained using the CACE, QACE [21], and ACD [22] models and experiment [7].

Moreover, it can be seen that the QACE [21] and ACD [22] models both show quantum effect contributions. Meanwhile, our obtained result reaches zero as the temperature reaches zero, so the CACE model is unsuitable in the low-temperature region because this model only uses classical statistical theory [19] in calculations. However, the CACE model still works effectively at temperatures that are not too low (T > θ_E), so our obtained result can be used well at room temperature.

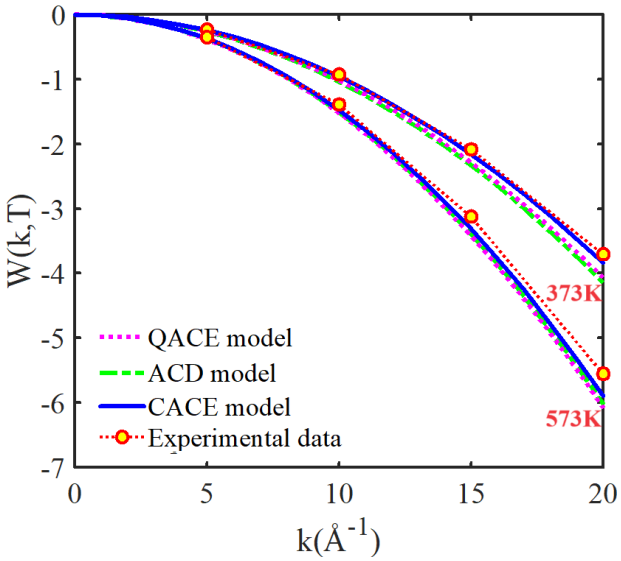

Fig. 6. The influence of temperature change on the XAFS DW factor of Mo is obtained using the CACE, QACE [21], and ACD [22] models and experimental data [7].

The anharmonic XAFS DW factor $W(T,k)$ of Mo at 373 K and 573 K and in a range from 0 to 20 Å is represented in Fig. 6. Herein, our obtained results using the CACE model are calculated by Eq. (12), other obtained results are calculated by Eq. (2), with the temperature-dependent second XAFS cumulant determined using the QACE [21], and ACD [22] models and experiment [7]. It can be seen that our results agree with those obtained using the QACE [21] and ACD [22] models and experimental data [7], especially at high temperatures and in the small wavenumber region. Moreover, the values of the XAFS DW factor decrease with increasing temperature *T* and decrease with fast-increasing wavenumber *k*. For example, the obtained results using the CACE model, QACE model, ACD model, and experimental data at $T \approx 373$ K and k = 10 Å are $W \approx -0.9$, $W \approx -1.0$ [21], $W \approx -1.0$ [22], and $W \approx -0.9$ Å^2 [7], respectively. Meanwhile, The respective obtained results are $T \approx 573$ K and k = 20 Å are $W \approx -5.9$, $W \approx -6.1$ [21], $W \approx -6.0$ [22], and $W \approx -5.6$ Å^2 [7], respectively. This is because the XAFS DW factor is an inverse function of the wavenumber k and second XAFS cumulant, in which this cumulant increases with increasing temperature *T*.

4. CONCLUSION

In this work, we have successfully applied the CACE model to calculate the temperature-dependent XAFS DW

factor of Mo. The obtained expression can satisfy all of their fundamental properties in the temperature-dependent. The anharmonic XAFS DW factor decreases with increasing temperature *T*. It means that the XAFS amplitude decreases more strongly at higher temperatures. These results can also describe the influence of anharmonic effects at high temperatures and the influence of quantum effects at low temperatures. The good agreement between our numerical results of Mo and those obtained using the QACE and ACD models and experimental data at various temperatures shows the effectiveness of the present model. This model can be applied to analyze the experimental XAFS data of other BCC metals from above absolute zero temperature to just before the melting point.

ACKNOWLEDGMENTS

The author would like to thank Assoc. Prof. N.B. Duc for their helpful comments. This work was supported by the Tan Trao University, Tuyen Quang, Vietnam.

REFERENCES

1. P. Fornasini, R. Grisenti, M. Dapiaggi, G. Agostini, and T. Miyanaga, Nearest-neighbour distribution of distances in crystals from extended X-ray absorption fine structure, Journal of Chemical Physics 147 (2017) 044503.
2. P. Eisenberger and G.S. Brown, The study of disordered systems by XAFS: Limitations, Solid State Communications 29 (1979) 481-484.
3. G. Dalba, P. Fornasini, and M. Grazioli, Local disorder in crystalline and amorphous germanium, Physical Review B 52 (1995) 11034-11043.
4. P. Fornasini and R. Grisenti, On XAFS Debye-Waller factor and recent advances, Journal of Synchrotron Radiation 22 (2015) 1242-1257.
5. P.B. Coffman, The Rise of a New Metal: The Growth and Success of the Climax Molybdenum Company, The Journal of Business of the University of Chicago 10 (1937) 30-45.
6. J. Emsley, Nature's Building Blocks. Oxford: Oxford University Press, 2001.
7. I.V. Pirog and T.I. Nedoseikina, Study of effective pair potentials in cubic metals, Physica B 334 (2003) 123-129.
8. T.S. Tien, N.V. Hung, N.T. Tuan, N.V. Nam, N.Q. An, N.T.M. Thuy, V.T.K. Lien, N.V. Nghia, High-order EXAFS cumulants of diamond crystals based on a classical anharmonic correlated Einstein model, Journal of Physics and Chemistry of Solids 134 (2019) 307-312.
9. T.S. Tien, Temperature-Dependent EXAFS Debye-Waller Factor of Distorted HCP Crystals, Journal of the Physical Society of Japan 91 (2022) 054703.
10. M. Newville, Fundamentals of XAFS, Reviews in Mineralogy & Geochemistry 78 (2014) 33-74.
11. R.B. Greegor and F.W. Lytle, Extended x-ray absorption fine structure determination of thermal disorder in Cu: Comparison of theory and experiment, Physical Review B 20 (1979) 4902-4907.
12. N.V. Hung, C.S. Thang, N.B. Duc, D.Q. Vuong, and T.S. Tien, Temperature dependence of theoretical and experimental Debye-Waller factors, thermal expansion and XAFS of metallic Zinc, Physica B: Condensed Matter 21 (2017) 198-203.
13. T. Fujikawa and T. Miyanaga, Quantum Statistical Approach to Debye-Waller Factors in EXAFS, EELS and ARXPS. I. Anharmonic Contribution in Plane-Wave Approximation, Journal of the Physical Society of Japan 62 (1993) 4108-4122.
14. T. Yokoyama, K. Kobayashi, T. Ohta, and A. Ugawa, Anharmonic interatomic potentials of diatomic and linear triatomic molecules studied by extended x-ray-absorption fine structure, Physical Review B 53 (1996) 6111-6122.
15. N.V. Hung and J.J. Rehr, Anharmonic correlated Einstein-model Debye-Waller factors, Physical Review B 56 (1997) 43-46.
16. R.V. Parish, The Metallic Elements, New York: Longman, 1977.
17. L.A. Girifalco and V.G. Weizer, Application of the Morse Potential Function to Cubic Metals, Physical Review 114 (1959) 687-690.
18. N.V. Hung, T.S. Tien, N.B. Duc, D.Q. Vuong, High-order expanded XAFS Debye - Waller factors of HCP crystals based on classical anharmonic correlated Einstein model, Modern Physics Letters B 28 (2014) 1450174.
19. E.A. Stern, P. Livins, and Z. Zhang, Thermal vibration and melting from a local perspective, Physical Review B 43 (1991) 8850-8860.
20. NW. Ashcroft and ND. Mermin, Solid State Physics, New York: Holt-Rinehart & Winston, 1976.
21. T.S. Tien, Extending quantum anharmonic correlated Einstein model in studies of anharmonic EXAFS Debye–Waller factor of BCC structure metals, European Physical Journal Plus 137 (2022) 1009.
22. N.V. Hung, T.T. Hue, H.D. Khoa, and D.Q. Vuong, Anharmonic correlated Debye model high-order expanded interatomic effective potential and Debye-Waller factors of bcc crystals, Physica B 503 (2016) 174–178.